

# Evaluation of the potential for greenhouse gas (CO<sub>2</sub>, CH<sub>4</sub>) emissions in the southern São Paulo coastal region, Cananéia-Iguape system

Elaine C. Araujo<sup>1\*</sup>, Thais Correa<sup>1</sup>, Izabel da S. Andrade<sup>1</sup>, Fernanda de M. Macedo<sup>4</sup>,  
Marcia T. Marques<sup>3</sup>, Thais Andrade<sup>1</sup>, Carlos Eduardo Souto-Oliveira<sup>3</sup>, Elisabete S. Braga<sup>2</sup>,  
Maria de F. Andrade<sup>3</sup>, Eduardo Landulfo<sup>1</sup>

<sup>1</sup> Instituto de Pesquisas Energéticas e Nucleares (Avenida Professor Lineu Prestes, 2242 – 05508-000 – São Paulo – SP – Brazil).

<sup>2</sup> Instituto de Oceanografia – Universidade de São Paulo (Praça do Oceanográfico, 191 – 05508-120 – São Paulo – SP – Brazil).

<sup>3</sup> Instituto de Astronomia, Geofísica e Ciências Atmosféricas – Universidade de São Paulo (Rua do Matão, 1226 – 05508-090 – São Paulo – SP – Brazil).

<sup>4</sup> Faculdade de Tecnologia do Estado de São Paulo (Praça 19 de janeiro, 144 – 11700-100 – Praia Grande – SP – Brazil).

\* Corresponding author: [elaine.c.araujo@usp.br](mailto:elaine.c.araujo@usp.br)

## ABSTRACT

The emissions of CH<sub>4</sub> and CO<sub>2</sub>, the primary greenhouse gases, have a significant impact on radiative forcing. This study investigated these gases along the Cananéia-Iguape estuarine system on the southern coast of the State of São Paulo, Brazil, which is a mangrove region characterized by low anthropogenic impact and a sparse population. As such, this area provides an ideal location for identifying natural emissions and background concentrations. The data for this study were collected using a portable gas analyzer (LGR-ICOS™ GLA131), known for its high sensitivity and precision in detecting gases, mounted on a research boat. The results obtained were promising for both gases. A small variability in CH<sub>4</sub> concentrations was observed along the route, ranging from 1.84 ppm to 1.95 ppm, while CO<sub>2</sub> showed greater variation in values obtained during routes, ranging from approximately 411 ppm to 575 ppm. This study underscores the importance of investigating areas with minimal environmental impact. Together with future analyses, this research should help improve Greenhouse Gas (GHG) inventories in Brazil by providing valuable baseline data for comparisons with more impacted areas.

**Keywords:** Methane, Carbon dioxide, Estuary, GHG, Microportable gas analyzers

## INTRODUCTION

Coastal areas represent only 7% of the total ocean surface but play an important role in biogeochemical cycles in continents, atmosphere,

and oceans (Burgos et al., 2018). Estuaries (the interface of freshwater inputs with saline water) are defined as semi-closed regions connecting the ocean to terrestrial drainage waters. These regions suffer a great influence of tidal variability, which directly impacts the biological development of the region (Borges et al., 2005). Estuaries are dynamic ecosystems and have one of the largest biological productions in the world, showing wide biodiversity and receiving an enormous amount of organic and

Submitted: 29-Aug-2022

Approved: 10-Feb-2024

Editor: Rubens Lopes



© 2024 The authors. This is an open access article distributed under the terms of the Creative Commons license.

inorganic matter, such as dissolved and particulate carbon (C), nitrogen (N), phosphorus (P), and silica ( $\text{SiO}_2$ ), which come from fresh water and undergo numerous transformations in the estuaries before being transferred to the coastal area.

Estuarine ecosystems are more metabolically active than other parts of the ocean. Thus, most estuaries have been reported as a source of  $\text{CO}_2$  (Borges et al., 2005), and emit carbon to the atmosphere in the form of carbon dioxide ( $\text{CO}_2$ ) and methane ( $\text{CH}_4$ ), two important greenhouse gasses with a considerable increase in concentration due to anthropogenic emissions since pre-industrial times. According to the IPCC 2013, carbon dioxide rose from 278 ppm in 1750 to 390.5 ppm in 2011, and methane, which is the second largest greenhouse gas responsible for radiative forcing, increased from 0.722 ppm in 1750 to 1.8 ppm in 2011 (Ferretti et al., 2005; Montzka et al., 2011; Stocker et al., 2013).

In 2019, detected  $\text{CO}_2$  concentrations were the highest recorded in at least two million years, and  $\text{CH}_4$  concentrations were the highest in at least 800,000 years. Since 1750, increases in  $\text{CO}_2$  (47%) and  $\text{CH}_4$  (156%) concentrations far exceed those observed in natural atmospheric changes in glacial and interglacial periods (IPCC, 2023).

Due to this increase in the concentration of these gasses and their great potential to interfere with radiative forcing during the last decade, GHG dynamics have been further investigated in various environments, which also include coastal areas, making estuaries very promising regions for GHG studies (Borges and Abril, 2011). As far as methane is concerned, the spatial distribution of  $\text{CH}_4$  concentrations in some estuaries is partially controlled by the entry of freshwater. Freshwater, with a high concentration of  $\text{CH}_4$ , mixes with seawater (which has low concentrations of  $\text{CH}_4$ ), making it responsible for the methane concentrations in coastal regions (de Angelis and Lilley, 1987; Upstill-Goddard et al., 2000; Middelburg et al., 2002). This methane dissolved in the freshwater column (90%) is lost at the entrance of the estuary to the atmosphere during its transport, with only a small fraction being oxidized in the

water column (Upstill-Goddard et al. 2000; Abril and Iversen 2002).

This study describes the exploratory analyses conducted in the Cananéia-Iguape estuarine system on the southern coast of São Paulo State, Brazil, a region of high biophysical complexity surrounded by mangroves, marine, and river plains whose marine sediments are reworked by rivers and added to other sediments from the interior of the continent (Ross and Moroz, 1997) and Ross (2002). It is one of the largest breeding sites of marine and terrestrial species in the South Atlantic (MMA, 2006), consisting of a system of four water bodies around four islands: Comprida, Cananéia, Cardoso, and Iguape (Araujo et al., 2005). According to Carlos and Hariri (2018), the circulation in the estuary Cananéia-Iguape is strongly influenced by the tide that penetrates Cananéia and Icapara bars, in addition to the contribution of fresh water from rivers. On some occasions, this circulation can be affected by several variables such as astronomical tide, fluvial discharge from Ribeira de Iguape, salinity variability, the action of winds, and seasonal variation of the surface temperature of the water. Within this context, vessel routes throughout the estuarine complex Cananéia-Iguape were performed to detect  $\text{CO}_2$  and  $\text{CH}_4$  by spectroscopy using a portable gas analyzer – Microportable Greenhouse Gas Analyzers (LGR ICOS™ GLA Series).

## METHODS

The data were obtained during a three-day campaign that took place in the region of Cananéia, on the southern coast of São Paulo State. The region has 2,450 km<sup>2</sup> of a wide estuary with 200 km<sup>2</sup> of well-preserved mangroves and a basin spanning 23,350 km<sup>2</sup>. The region has a low anthropic impact as part of the Atlantic Forest Biosphere Reserve and the World Heritage Site, recognized by UNESCO in 1991 and 1999, respectively (Santos and Tatto, 2008). The population of this region totals around 51,800 inhabitants (IBGE, 2022), most of whom is concentrated in the region of the Iguape municipality in the northern area of the estuary. Measurements were performed

uninterruptedly from 11/23/2021 to 11/25/2021 onboard the vessel *Albacora*, supplied by IOUSP. The route of the campaign started every day at the Pier of IOUSP Research Base “Dr. João de Paiva

Carvalho” and the vessel travelled predetermined routes for each campaign day to traverse the entire estuary. Figure 1 shows the Cananéia-Iguape estuarine complex.

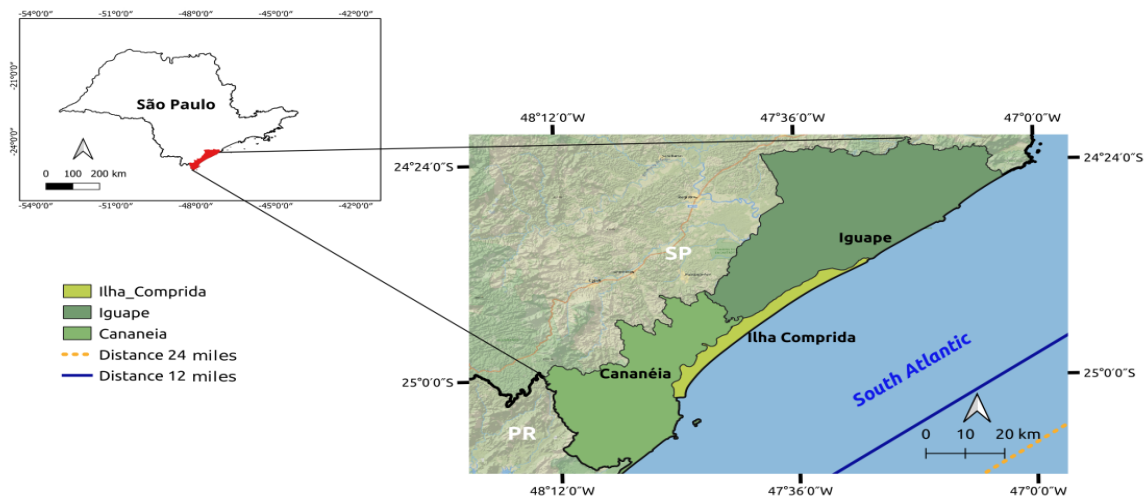


**Figure 1.** Estuarine Complex Cananéia-Iguape. Scale 1:200000. (November 10, 2023). Using: QGIS [GIS software]. Version 3.28.11. QGIS Geographic Information System. Open Source Geospatial Foundation Project.

For data collection, a portable gas analyzer - Microportable Greenhouse Gas Analyzers (LGR-ICOS™ GLA Series) was used. This instrument has high sensitivity, resulting in a very fast gas flow response time (1 second). The Microportable Greenhouse Gas Analyzers LGR-ICOS, based on the Off-Axis Integrated Cavity Output Spectroscopy (OA-ICOS), a technique that is widely utilized for gas detection due to its rapid response, high sensitivity, and stability (Krishnan et al., 2009; Sebastien et al., 2020), obtain a precision of <math><0.9\text{ ppb}</math> (1 second) for  $\text{CH}_4$  and <math><350\text{ ppb}</math> for  $\text{CO}_2$  (1 second). These analyzers boast measurement rates ranging from 0.01 to 10 Hz and accommodate  $\text{CH}_4$  concentrations from 0.01 to 100 ppm and  $\text{CO}_2$  concentrations from 10 to 20,000 ppm, respectively. The laser wavelength chosen for analysis is determined by the absorption characteristics of the measured gas. This determination is achieved by combining the

spectra with the temperature and pressure of the measured gas, the effective optical path length, and the known strength of the absorption line (ABB Inc., 2020). Its operation resembles that of non-portable gas analysis equipment, such as Cavity ring-down Spectroscopy. Figure 2 shows a diagram for the air flux in the portable gas analyzers. The gas sample enters through the INLET (IN), and after that, the gas goes through a series of filters, the first of which a “screen filter” of  $5\ \mu\text{m}$ . Just after passing through the pressure adjustment that keeps the pressure at a specific setting point, the gas passes through another filter that has an efficiency  $> 95\%$  and removes particles that are  $0.01\text{-}\mu\text{m}$  in diameter or larger. Finally, the gas passes through the optical cell valve, in which the transmission of light through the cavity is detected and the signal is digitized, analyzed, and stored in an internal computer. After this step, the sample exits through the outlet valve port (OUT).

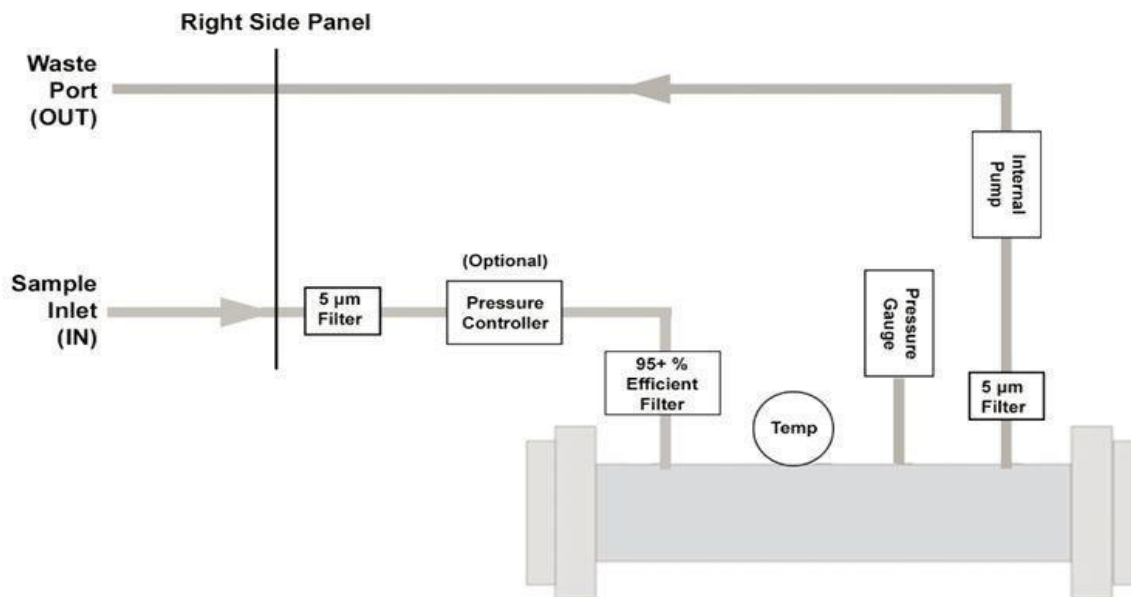


**Figure 2.** Plumbing Diagram Microportable Greenhouse Gas Analyzers (LGR-ICOS™ GLA Series)- adapted from User Manual GLA 131 series, 2020.

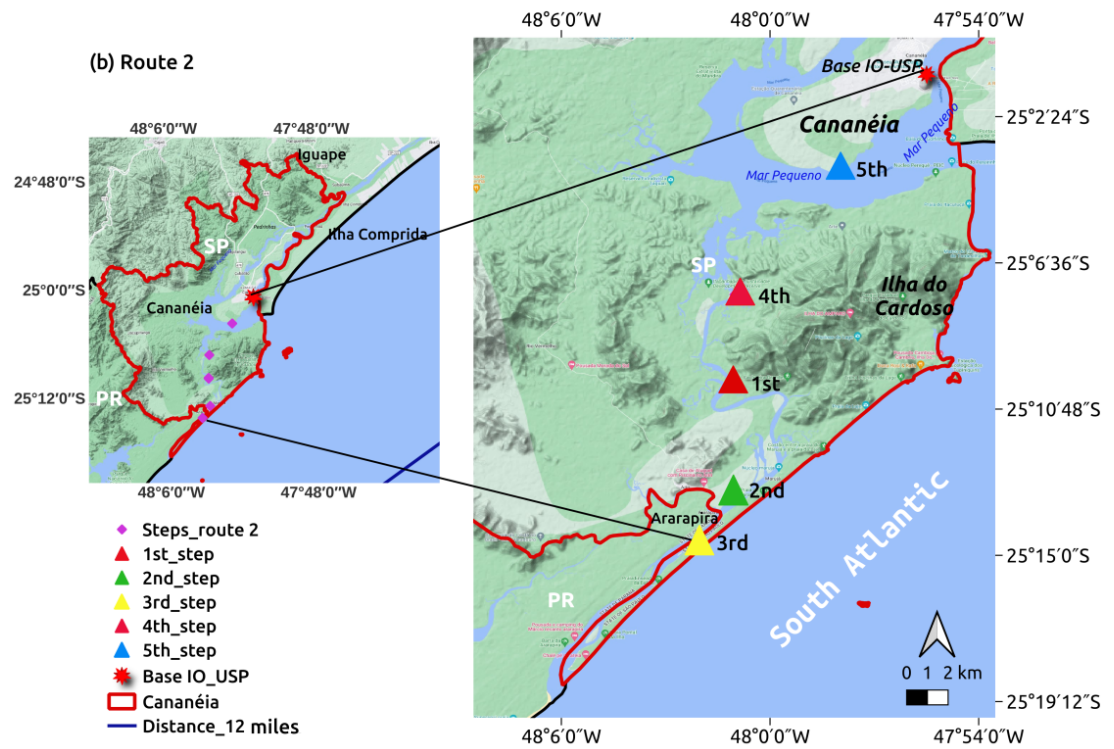
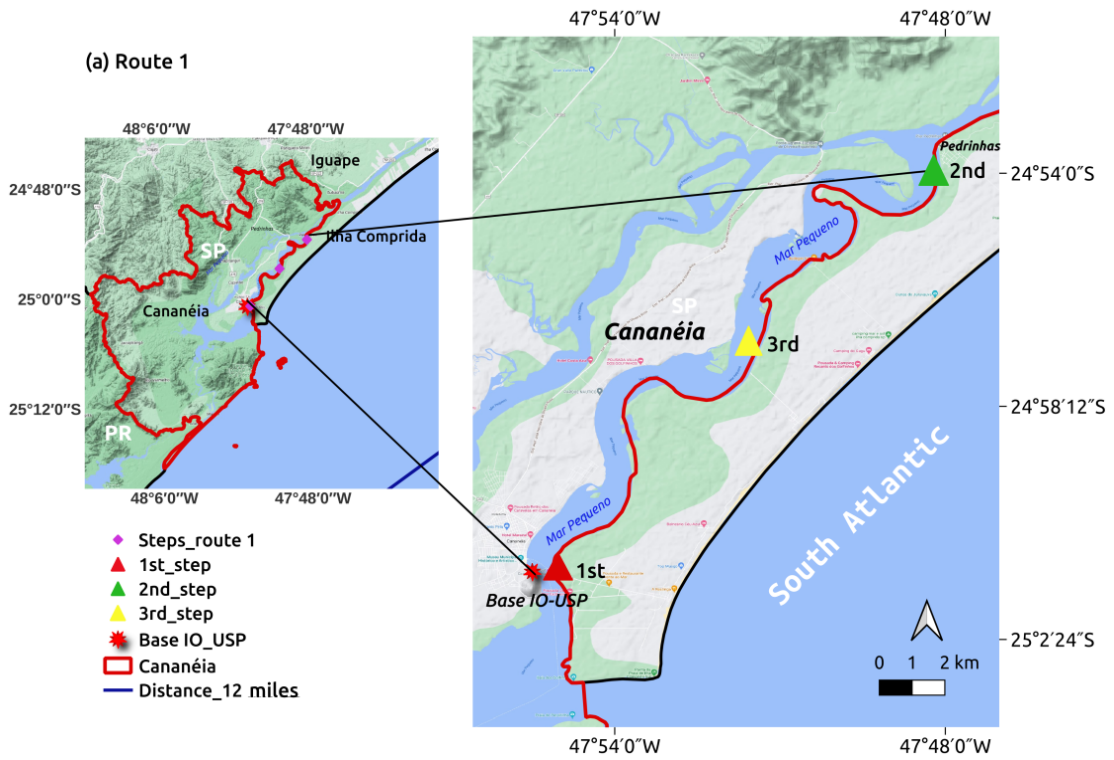
Some important adjustments were made to improve the quality of the data in addition to the equipment filter system. A Teflon tube of  $\frac{1}{4}$  was coupled to the INLET, which extended up to about 3 meters above sea level and was positioned above the cabin of the captain of the vessel at half ship. At the end of this tube a PFA 47-mm Savillex filter holder was attached, and inside this support a Zefluor membrane of  $2.0 \mu\text{m}$  was used. As a first step, a silica filter was installed between the INLET and the cabin support to minimize the impact of moisture on data acquisition. The configuration of the equipment was programmed so that the data were obtained every second in the local time, thus obtaining a representative data set.

For statistical analyses, the Python programming language (version 3.8) and its scientific libraries, such as Pandas for data manipulation, NumPy for numerical calculations, and Matplotlib for visualization of the results, were used. Using this platform, analyses of the raw data were carried out by boxplot which sought to show the origin of most of the data obtained in each day of the campaign. For a second analysis, a minimum and maximum

limit were also inserted by calculating Interquartile Ranges (IQR), which is the difference between the Third (Q3) and the First Quartile (Q1) - representing the amplitude of the interval in which the central half of the data is concentrated, ignoring the extremes. In view of the values in this analysis, the data set for the inline graphs was separated in averages of every 180 seconds from the measured raw data (1 per second) and limited to 1.8 to 2.0 ppm for methane and 400 to 600 ppm for carbon dioxide.

## RESULTS

To complete the entire journey throughout the Cananéia-Iguape estuarine complex, the campaign was divided into three routes. The first day campaign was to be at the nearest location to Cananéia Island, on the second day the journey was around South of Cananéia around the Cardoso island up to the border with Paraná state, and on the last day the route traversed Iguape arriving near the mouth of Icapara. Table 1 further details these three days of campaign and Figure 3 shows the route on each day of the campaign, from 11/23/2021 to 11/25/2021.



continued



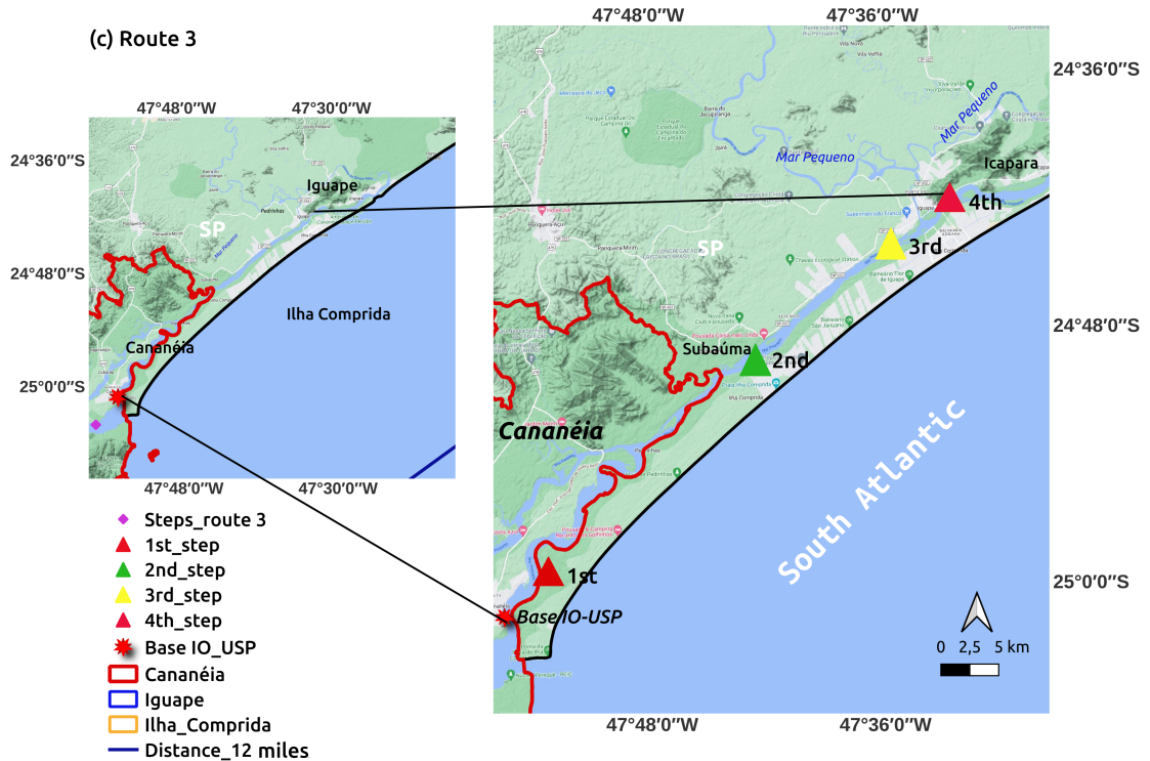


**Figure 3.** Routes undertaken during the Albacora II campaign in the Cananéia-Iguape estuary system from November 23<sup>rd</sup> to November 25<sup>th</sup>. The three routes show the paths for the campaign, its steps, and vessel. Route 1 - Figure (a): Scale 1:90000; Route 2 - Figure (b): Scale 1:140000; Route 3 - Figure (c): Scale 1:330000. (November 10, 2023). Using: QGIS [GIS software]. Version 3.28.11. QGIS Geographic Information System. Open Source Geospatial Foundation Project.

**Table 1.** Details of Campaign Albacora II

Routes	Date	Start	Return	Ending	Details
<b>1 - Cananéia - Pedrinhas</b>	11-23-2021	9 am (UTC-3)	5 pm (UTC-3)	11 pm (UTC-3)	During the course, the boat stopped at some points, the first point near the base of IOUSP and the second in the middle of the way to Pedrinhas Village, which was the last stop of this route.
<b>2 – Ilha do Cardoso - Ararapira</b>	11-24-2021	7 am (UTC-3)	5 pm (UTC-3)	11 pm (UTC-3)	The second day had five stops, which passed near the bar of Cananéia, Cardoso Island, going to the border of Paraná State near Barra de Ararapira.
<b>3 - Iguape</b>	11-25-2021	7 am (UTC-3)	7 pm (UTC-3)	11 pm (UTC-3)	On the last day, the journey headed toward Iguape. It stopped four times next to three regions: Cananéia, Subaúma, and Barra de Icapara.

A preliminary and general analysis of the raw data showed that the concentrations for the Albacora II campaign have a data set with concentrations from ~1.84 to ~1.92 ppm for CH<sub>4</sub> and from ~410 to ~480 ppm for CO<sub>2</sub> (Figure 4). Results refer to the three days of the campaign.

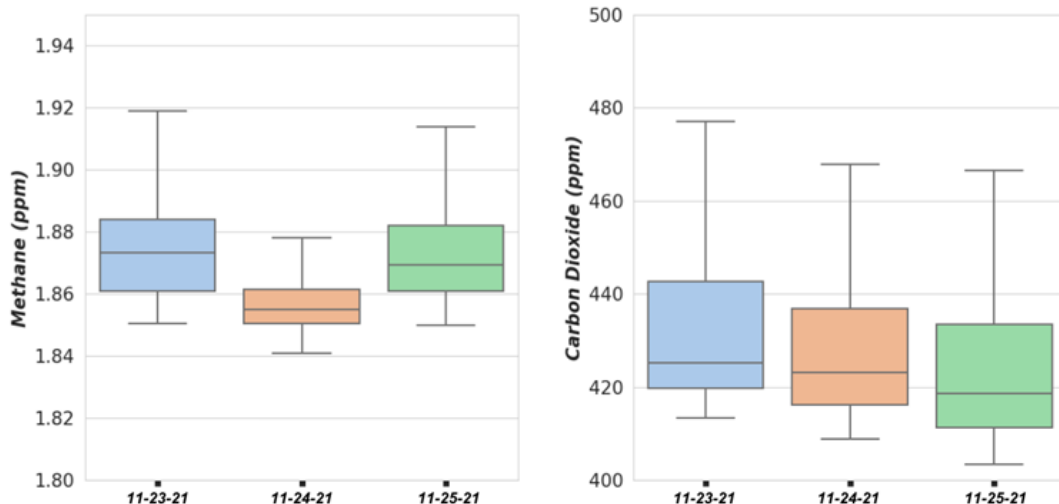


**Figure 4.** Boxplot of daily CO<sub>2</sub> and CH<sub>4</sub> concentrations.

Figures 5a and 5b show the variability of CO<sub>2</sub> and CH<sub>4</sub> data at different times for each campaign day within the interquartile range (IQR), which enable us to view data outside the central trend. The lines highlighted in both graphs show the maximum and minimum limits for the entire dataset on a measurement day. The blue line highlights the upper limit value and the red line highlights the lower limit obtained by calculating the IQR. For CO<sub>2</sub>, IQR totaled about 20.9 ppm, obtaining values of 387, 386, and 378 ppm for the minimum limits and of 475, 467, and 466 ppm (Figure 5b) for the maximum limit for November 23<sup>rd</sup>, 24<sup>th</sup>, and 25<sup>th</sup>, respectively. It is then possible to observe that most of the obtained dataset values exceed the lower limit determined by the IQR calculation since the minimum value of carbon dioxide for these dates was ~411 ppm. At some times, it is possible to observe that some outliers reach the value of about 575 ppm, exceeding the upper limit of the interquartile (475 ppm). For methane data, the IQR totaled 0.025 ppm, which shows a lower

variability in the obtained data, the lower limit for the CH<sub>4</sub> data totaled 1.83 ppm for all campaign days and the upper limit ranged from 1.88 to 1.92 ppm (Figure 5a), whereas methane concentrations for the measurement days, from ~1.84 to ~1.92 ppm, mostly within the minimum and maximum limits of the interquartile.

On the first day (November 23), the dataset refers to 14 measured hours and for the other days, November 24 and 25, the dataset spans 16 hours. The first day has a smaller dataset due to activities that began a little late. Table 1 shows the start and end of each campaign day.

The first route (Figure 3, route 1) occurred between Cananéia and Pedrinhas, starting at Base IOUSP – Cananéia, the oscillations for CH<sub>4</sub> remained from ~1.85 to ~1.92 ppm as most of the route found 1.85 ppm with some occasional peaks at ~1.9 ppm. When the vessel was returning to the IOUSP base, the methane concentration during the two-hour interval totaled ~1.9 ppm. Carbon dioxide oscillated from ~420 to ~550 ppm, this higher value occurred at the beginning of the route from around 10 am to 12 am, when the vessel was still in Cananéia. Moving toward the Pedrinha village the maximum value had a decreased to ~475 ppm, peaking near ~500 ppm only when it was near the base of IOUSP again (Figure 6).

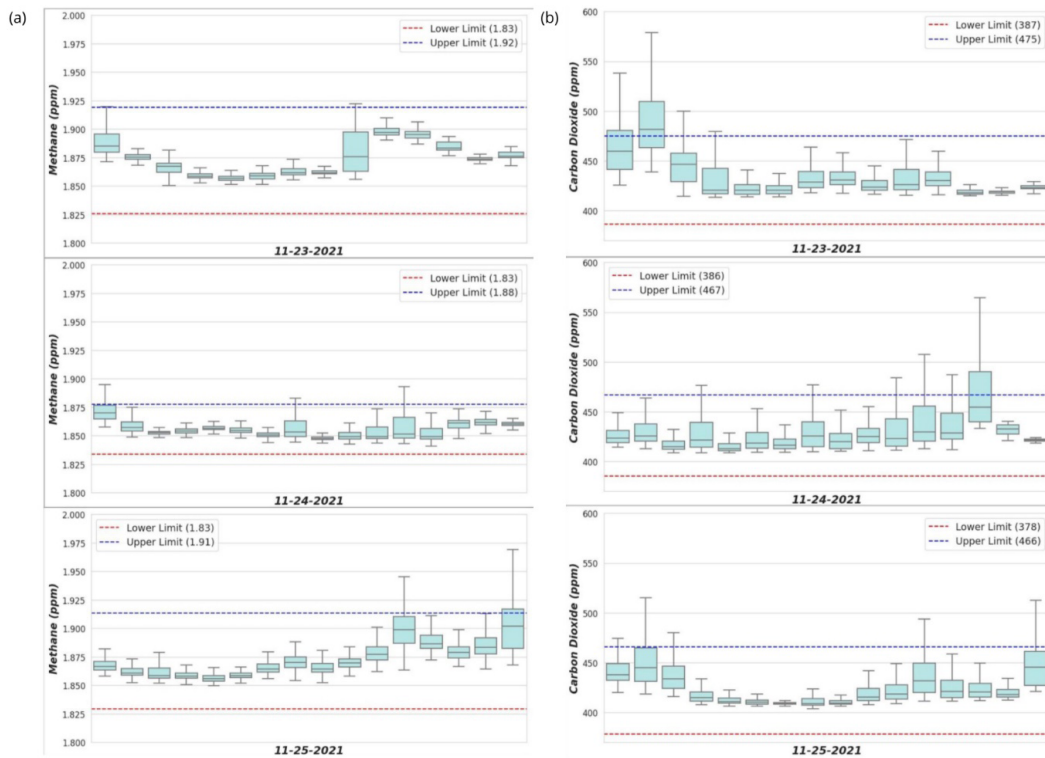


**Figure 5.** Boxplot for the daily data of CH<sub>4</sub> (a) and CO<sub>2</sub> (b) concentrations per hour. Data from this campaign were acquired at second intervals, as mentioned earlier. This resulted in significant variations in concentration due to the high accuracy of the equipment. For a more specific analysis, we excluded values that considerably exceeded the limits, restricting our analysis to a range of 1.8 to 2.0 ppm for methane and 400 to 600 ppm for carbon dioxide. Then, we applied an average every three-minute interval. Some points were highlighted in Figures 6, 7, and 8 at the moment the vessel approximately docked for collection of water samples, which are not included in this work. The points in general the vessel stood still for about an hour and the average hour concentration in these stops can be viewed in Table 2.

**Table 2.** Concentrations and standard deviations of CO<sub>2</sub> and CH<sub>4</sub> according to the hourly stops of the vessel in the three days of campaign.

Time (UTC-3)	Concentration CH <sub>4</sub>	Standard deviation - CH <sub>4</sub>	Concentration CO <sub>2</sub>	Standard deviation CO <sub>2</sub>	Latitude/Longitude
<b>Day 1– 11-23-21</b>					
10 am	1.88 ppm	0.002	490.62 ppm	35.09	25°1'S/ 47°55'W
3 pm	1.87 ppm	0.013	436.26 ppm	22.67	24°54'S/47°48'W
6 pm	1.90 ppm	0.005	438.04 ppm	27.67	24°57'S/47°51'W
<b>Day 2– 11-24-21</b>					
12 am	1.86 ppm	0.009	424.47 ppm	16.45	25°10'S/48° 1'W
2 pm	1.86 ppm	0.026	433.73 ppm	26.58	25°14'S/48° 2'W
4 pm	1.85 ppm	0.013	428.85 ppm	16.46	25°13'S/48° 1'W
6 pm	1.86 ppm	0.026	445.99 ppm	37.89	25° 7'S/48° 1'W
8 pm	1.86 ppm	0.005	470.04 ppm	38.05	25° 04'S/47° 58'W
<b>Day 3– 11-25-21</b>					
9 am	1.86 ppm	0.014	439.52 ppm	22.04	24°59'S/47°53'W
12 am	1.86 ppm	0.004	412.29 ppm	8.22	24°49'S/47°42'W
2 pm	1.87 ppm	0.007	411.77 ppm	7.81	24°44'S/47°35'W
5 pm	1.88 ppm	0.016	423.67 ppm	16.72	24°42'S/47°32'W



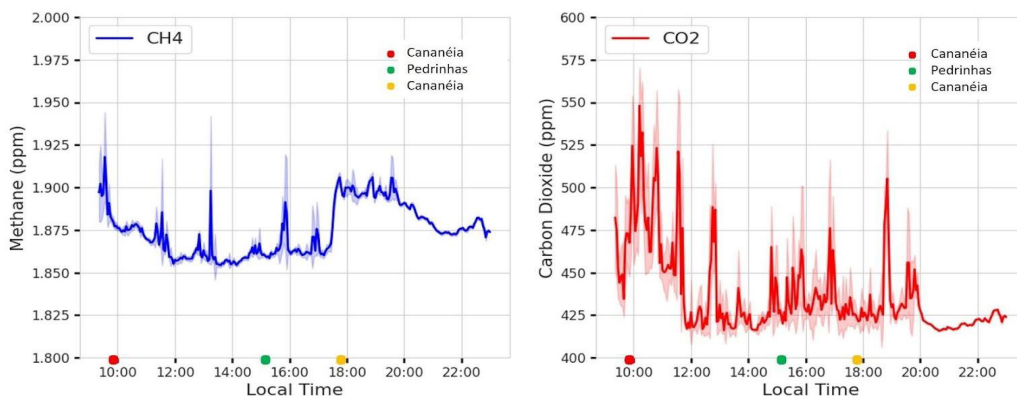


**Figure 6.** CO<sub>2</sub> and CH<sub>4</sub> three-minute average for November, 23. The blue and red lines indicate the values of methane and carbon dioxide concentrations, respectively, and the shadow in each figure represents the standard deviation.

Over the second day, sample values for methane remained almost constant from ~1.84 to ~1.88 ppm (Figure 7), except in three moments in which concentrations reached 1.9 ppm at about 3, 4 pm, and 6 pm (UTC-3). This route (Figure 3, route 2) headed further south the IOUSP base in Cananéia, in the vicinity of Cardoso Island to Ararapira, a sparsely populated village belonging

to the municipality of Guaraqueçaba (IBGE, 2022), near the border with Paraná State, Brazil. During these hours of navigation, carbon dioxide concentrations ranged from ~417 to ~550 ppm (Figure 7), mostly remaining from 420 to 450 ppm, only increasing (above 500 ppm) close to Cardoso Island and Barra de Cananéia, as can be seen in the last two points highlighted in Figure 7.

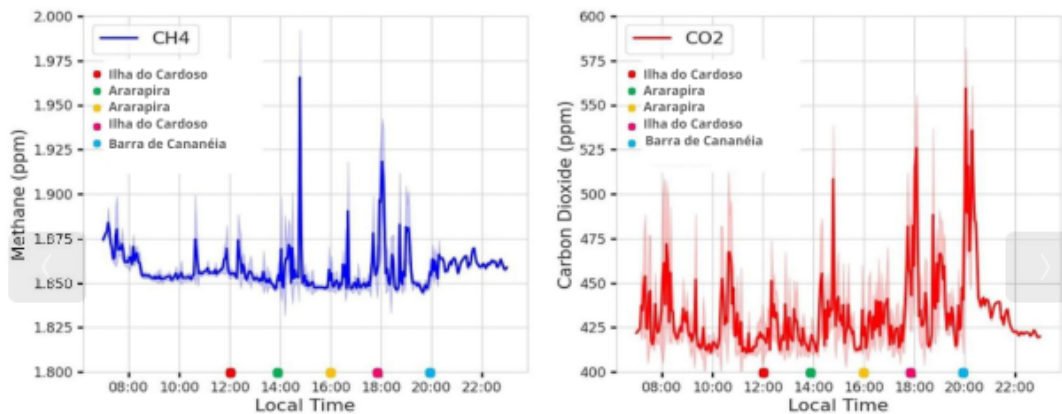


**Figure 7.** CO<sub>2</sub> and CH<sub>4</sub> three-minute average for November, 24. The blue and red lines indicate the values of methane and carbon dioxide concentrations, respectively, and the shadow in each figure represents the standard deviation.

In the northernmost region of the IOUSP Base, between Pedrinhas and Iguape, an exploration was conducted on November 25, 2021. Regarding CH<sub>4</sub> values, for the initial segment of the route, concentrations ranged from ~1.85 to ~1.88 ppm (Figure 8). As the vessel started its return journey to the IOUSP base, methane concentrations gradually

increased, with two peaks reaching ~1.95 ppm occurring from 9 to 11 pm, when the vessel was very close to the IOUSP base in Cananéia. It was observed that CO<sub>2</sub> values consistently remained below 450 ppm (Figure 8) for most of the journey from Cananéia to Iguape, from about 8 am to 5 pm (UTC-3). The lowest value in the analysis totaled

around 411 ppm near Subaúma (Figure 3, route 3) at about 12 am (UTC-3). It is worth noting that up to the departure time from the base point, the vessel recorded values ranging from ~425 to ~475 ppm (Figure 8). As the journey progressed, these values gradually decreased. When the boat

approached the Iguape region and returned to the IOUSP base in Cananéia (at around 5 pm), values began to increase again. However, average values generally remained below 475 ppm, peaking at almost 550 ppm near the IOUSP base at 11 pm (UTC-3), but this was an isolated occurrence.

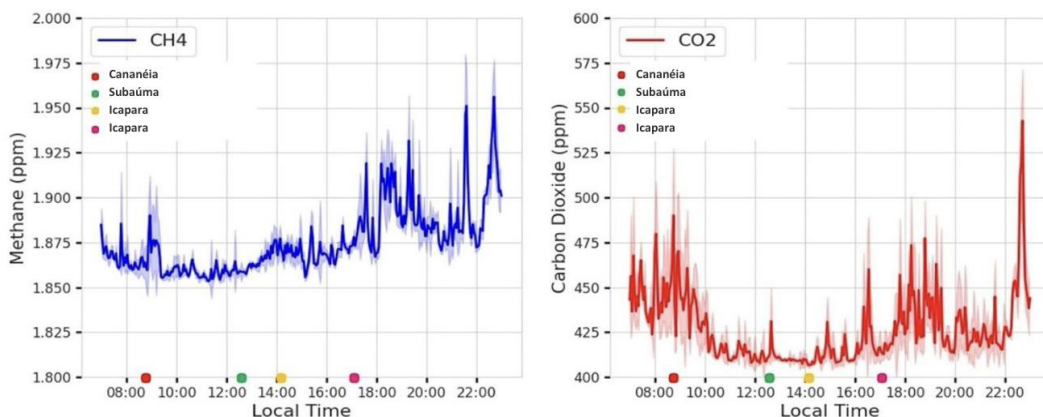


**Figure 8.** CO<sub>2</sub> and CH<sub>4</sub> three-minute average for November, 24. The blue and red lines indicate the values of methane and carbon dioxide concentrations, respectively, and the shadow in each figure represents the standard deviation.

## DISCUSSION

Wetlands are currently the primary natural contributor of atmospheric CH<sub>4</sub>, with emissions influenced by environmental variables such as soil temperature, water table depth, and vegetation cover and composition. All these factors are susceptible to the impacts of climate change. Calculations suggest that under climate change scenarios, heightened CH<sub>4</sub> emissions from wetlands may lead to an amplified radiative forcing effect (Kathleen et al., 2022). According to The Global Monitoring Division at the NOAA Earth System Research Laboratory, the monthly global trend of methane was 1.87 ppm in 2020. The CH<sub>4</sub> concentrations in the study area ranged from approximately 1.84 to 1.95 ppm, characterized as a basal concentration according to previous studies. The peak values observed in methane (CH<sub>4</sub>) measurements during the vessel steps, based on a three-minute average, ranged from 1.85 to 1.88 ppm (Table 2), showing little variation and remaining stable, similar to the value found by Lan et al. (2023) in the previous year of the campaign (1.87 ppm). This variability, although low, brings to light the discussion about the significant

increase in methane concentrations, as compared to previous studies showing values of 700 ppb in 1750 and 1745 ppb in 1998 (IPCC, 2013, 2021). It is known that the increase in the concentration of CH<sub>4</sub> may lead to an increase in the concentration of CO<sub>2</sub> in the region since tropospheric CH<sub>4</sub>, when oxidized, generates CO<sub>2</sub> (Kathleen et al., 2022).

A factor that may justify variations in CH<sub>4</sub> concentrations is biological activity, e.g., the balance between methanogenesis and methanotrophy, which is driven by highly variable microbiological and physical processes that depend on organic matter inputs, hydrodynamics, salinity, and temperature (Martens et al., 1998; Borges and Abril, 2011).

The CO<sub>2</sub> concentrations in this period ranged from 411 to 575 ppm (Figure 5b). Biological activity can justify this behavior since, according to Borges et al. (2005), the estuarine region can behave as a source of CO<sub>2</sub> emissions, rather than as a sink. According to the NOAA Earth System Research Laboratory in Mauna Loa, the expected values global for monthly average atmospheric concentrations of CO<sub>2</sub> were approximately 415 ppm in 2020 (NOAA, 2023), values close to the minimum concentration

of carbon dioxide (411 ppm) found during the campaign. The highest CO<sub>2</sub> values, approximately 575 ppm, were observed on the first and second days of the campaign (Figure 5b). However, these values are inconstant and, when averaged every 180 seconds, the highest concentration in these cases was approximately 550 ppm (Figures 6 and 7). These temporal variations may reflect the dynamic response of CO<sub>2</sub> concentrations to human activities, changes in weather conditions, and daily natural patterns. For example, spikes on the first two days may be associated with specific activities or environmental conditions during those periods.

The relation between the highest CO<sub>2</sub> values and its concentration during boat stops is evident. The highest CO<sub>2</sub> values during stops were recorded on the first two days of the campaign, namely at stop 1 of the first day, around 10 am, and in the last stop of the second day, around 8 pm (Table 2). This regularity implies that certain activities or conditions occurring during these periods could have played a role in the observed surges in CO<sub>2</sub> concentrations given the dynamic nature of estuarine ecosystems. Thus, the Cananéia-Iguape estuary is an interesting area of study because it is one of the main areas of preserved mangrove in Brazil (Brito et al., 2014). In this study, it was possible to measure the variability of methane and carbon dioxide concentrations in the atmosphere. All the data collected in this campaign point to the need for further *in situ* data on the atmosphere of CH<sub>4</sub> and CO<sub>2</sub> in preserved areas and those under anthropic influences. These analyses (better known as bottom-up analyses) are extremely relevant for the understanding of the emitting sources and the sinks that impact the climate changes (IPCC, 2023). This study, with its pioneering spirit of analyzing the atmosphere in such a complex estuarine region such as Cananéia-Iguape, significantly contributes to the observation of the behavior of a wetland and mangroves as a source or sink of greenhouse gas.

## CONCLUSION

GHG concentrations in the Cananéia-Iguape estuarine system showed significant variability within the studied micro-regions and should be

better evaluated and compared with other analyses carried out during the Albacora II campaign. As already pointed out, the biological activity in the region is very intense because the region has a high degree of environmental preservation. Studies in wetlands with low environmental impact may contribute to the improvement of GHG inventories in Brazil in the future. Moreover, such analyses in a region with low environmental impact enable us to build an instigating comparative panorama between natural emissions in diversified situations and the already observed anthropic emissions in more impacted regions and justify the continued development of this research. Finally, a factor that corroborates more extensive campaigns is the fact that this study pioneers the use of a Microportable Greenhouse Gas Analyzer to survey GHG data not only in the Cananéia-Iguape estuary region but also throughout Latin America.

## ACKNOWLEDGMENTS

We would like to thank the Oceanographic Institute for their support and knowledge shared during the Albacora II campaign and the Metroclima project. We also extend our gratitude to the Institute of Astronomy, Geophysics, and Atmospheric Sciences for their partnership and to FAPESP for financial support under projects n°16/18438-0 and 2020/16485-7, as well as to CAPES and CNPQ for the scholarships provided to our students (CAPES scholarships: 88887.473711/2020-00, 88887.464990/2019-00, and 88887.473416/2020-00; CNPQ scholarship: 131458/2023-0). Lastly, we thank the reviewer for their comments and questions, which were extremely important to the improvement of this and future research.

## AUTHOR CONTRIBUTIONS

E.C.A.; T.C.: Conceptualization; Methodology.

E.C.A.; I.S.A.: Software.

E.C.A.; I.S.A.; T.C.; F.M.M.: Formal analysis; Investigation.

E.C.A.: Validation; Writing — original draft preparation.

E.L.: Resources; Supervision.

T.A.; M.T.M.; C.E.S.; E.S.B.: Data curation.

I.S.A.; F.M.M.; T.C.; T.A.: Writing—review and editing.

E.L.; M.F.A.; E.S.B.: Project administration.

M.F.A.: Funding acquisition.

## REFERENCES

- ABB Inc. *User Manual OA-ICOS*. GLA131 Series Microportable Analyze. Zurich, 2020.
- Abril, G. & Iversen, N. 2002. Methane dynamics in a shallow non-tidal estuary (Randers Fjord, Denmark). *Marine ecology progress series*, 230, 171–181. DOI: <https://doi.org/10.3354/meps230171>
- Araújo, C.O., Souza, F.M., Arzolla, F.A.R.D.P., Franco, G.A.D.C., Baitello, J.B., Toniato, M.T.Z., Ivanauskas, N.M., Aguiar, O.T. & Cielo Filho, R. 2005. *Módulo Biodiversidade: Relatório Vegetação. Plano de Manejo do Parque Estadual da Serra do Mar*. São Paulo, Instituto Florestal do Estado de São Paulo.
- Borges, A. V. & Abril, G. 2011. Carbon dioxide and methane dynamics in estuaries. In: Wolanski, E. & McLusky, D. (eds.). *Treatise on estuarine and coastal science* (pp. 119–161). Amsterdam: Academic Press. DOI: <https://doi.org/10.1016/B978-0-12-374711-2.00504-0>
- Borges, A. V., DeLille, B. & Frankignoulle, M. 2005. Budgeting sinks and sources of CO<sub>2</sub> in the coastal ocean: Diversity of ecosystems counts. *Geophysical research letters*, 32(14), L14601. DOI: <https://doi.org/10.1029/2005GL023053>.
- Brito, D. D., Milanelli, J. C. C., Riedel, P. S. & Wieczorek, A. 2014. *Sensibilidade do litoral paulista a derramamentos de Petróleo - um atlas em escala de detalhe*. Rio Claro, UNESP.
- Burgos, M., Ortega, T. & Forja, J. 2018. Carbon dioxide and methane dynamics in three coastal systems of Cadiz Bay (SW Spain). *Estuaries and Coasts*, 41(4), 1069–1088. DOI: <https://doi.org/10.1007/s12237-017-0330-2>
- Carlos, A. F. & Harari, J. 2018. Interação da hidrodinâmica com o gerenciamento costeiro e pesqueiro no Litoral Sul de São Paulo. In: Sinisgalli, P. A. A. & Jacobi, P. R. (orgs.). *Caminhos do conhecimento em interdisciplinaridade e meio ambiente* (vol. 1; pp. 15-37). São Paulo: Instituto de Energia e Ambiente da Universidade de São Paulo.
- De Angelis, M. A. & Lilley, M. D. 1987. Methane in surface waters of Oregon estuaries and rivers. *Limnology and Oceanography*, 32(3), 716–722. DOI: <https://doi.org/10.4319/lo.1987.32.3.0716>
- Ferretti, D. F., Miller, J. B., White, J. W. C., Etheridge, D. M., Lassey, K. R., Lowe, D. C., Macfarling Meure, C. M., Dreier, M. F., Trudinger, C. M., van Ommen & Langenfelds, R. L. 2005. Unexpected changes to the global methane budget over the past 2000 years. *science*, 309(5741), 1714-1717. doi.org/10.1126/science.1115193
- IBGE (Instituto Brasileiro de Geografia e Estatística). 2022. *Censo 2022: Panorama*. Indicadores. Available from: <https://censo2022.ibge.gov.br/panorama/indicadores.html?localidade=3509908>. Access date: 2023 Aug 14.
- Stocker, T.F., Qin, D., Plattner, G.-K., Tignor, M., Allen, S.K., Boschung, J., Nauels, A., Xia, Y., Bex, V. & Midgley, P.M. (eds.). 2013. *Climate Change 2013: The Physical Science Basis*. Contribution of Working Group I to the Fifth Assessment Report of the Intergovernmental Panel on Climate Change. Geneva, IPCC.
- IPCC (Intergovernmental Panel on Climate Change). 2023. *Climate Change 2021: The Physical Science Basis*. Contribution of Working Group I to the Sixth Assessment Report of the Intergovernmental Panel on Climate Change. Cambridge, Cambridge University Press. <https://doi.org/10.1017/9781009157896>.
- Kathleen, A. M., Charlotte, U., Ludmila, W. & Tim, B. 2022. Beyond CO<sub>2</sub> equivalence: The impacts of methane on climate, ecosystems, and health. *Environmental Science and Policy*, 134, 127–136. DOI: <https://doi.org/10.1016/j.envsci.2022.03.027>.
- Krishnan, R. P., David, I. R., Mark, G. A., Alan, M. G. & Terence, H. R. 2009. Off-axis integrated cavity output spectroscopy with a mid-infrared interband cascade laser for real-time breath ethane measurements. *Applied optics*, 48(4), B73–B79. <https://doi.org/10.1364/AO.48.000B73>
- Lan, X., Thoning, K. W. & Dlugokencky, E. J. 2023. *Trends in globally-averaged CH<sub>4</sub>, N<sub>2</sub>O, and SF<sub>6</sub>*. Boulder, NOAA Global Monitoring Laboratory measurements. <https://doi.org/10.15138/P8XG-AA10>
- Martens, C. S., Albert, D. B., & Alperin, M. J. 1998. Biogeochemical processes controlling methane in gassy coastal sediments—Part 1. A model coupling organic matter flux to gas production, oxidation and transport. *Continental Shelf Research*, 18(14-15), 1741–1770. [https://doi.org/10.1016/S0278-4343\(98\)00056-9](https://doi.org/10.1016/S0278-4343(98)00056-9)
- Middelburg, J. J., Nieuwenhuize, J., Iversen, N., Høgh, N., De Wilde, H., Helder, W., Seifert, R. & Christof, O. 2002. Methane distribution in European tidal estuaries. *Biogeochemistry*, 59(1), 95–119. <https://doi.org/10.1023/A:1015515130419>
- MMA (Ministério do Meio Ambiente). 2006. *Portaria n. 150, de 8 de maio de 2006*. Brasília, DF, Ministério do Meio Ambiente.
- Montzka, S. A., Dlugokencky, E. J. & Butler, J. H. 2011. Non-CO<sub>2</sub> greenhouse gases and climate change. *Nature*, 476(7358), 43–50. doi.org/10.1038/nature10322
- NOAA (National Oceanic and Atmospheric Administration – Global Monitoring Laboratory). [2010]. *Trends in Global Carbon Dioxide*. Boulder, NOAA. Available from: <https://gml.noaa.gov/ccgg/trends/global.html>. Access date: 2023 Aug 14.
- Ross, J. L. S. & Moroz, I. C. 1997. *Mapa Geomorfológico do Estado de São Paulo: escala 1:500.000*. São Paulo, FAPESP.
- Ross, J. L. S. 2002. A morfogênese da bacia do Ribeira do Iguape e os sistemas ambientais. *GEOUSP – Espaço e Tempo*, 12, 21–46.
- Santos K. M. S. & Tatto N. 2008 *Agenda Socioambiental de Comunidades Quilombolas do Vale do Ribeira*. São Paulo, Instituto Socioambiental.
- Sebastien, A., Felix, V., Colin, A., Sajjan, H., Emily, K., Juliette, L., Christopher, L., Nasrin, M. P., Jaden, L. P. & Debra, W. 2020. Investigation of the Spatial Distribution of Methane Sources in the Greater Toronto Area Using Mobile Gas Monitoring Systems. *Environmental Science and Technology*, 54, 15671–15679. DOI: <https://doi.org/10.1021/acs.est.0c05386>
- Upstill-Goddard, R. C., Barnes, J., Frost, T., Punshon, S. & Owens, N. J. 2000. Methane in the southern North Sea: Low-salinity inputs, estuarine removal, and atmospheric flux. *Global Biogeochemical Cycles*, 14(4), 1205-1217. DOI: <https://doi.org/10.1029/1999GB001236>